IEEE Access
Multidisciplinary ⋮ Rapid Review ⋮ Open Access Journal

Received 24 March 2023, accepted 7 April 2023, date of publication 18 April 2023, date of current version 21 April 2023.

*Digital Object Identifier 10.1109/ACCESS.2023.3268086*

RESEARCH ARTICLE

# Deep Learning for Compressed Sensing-Based Blade Vibration Reconstruction From Sub-Sampled Tip-Timing Signals

**ZHONGSHENG CHEN[1], (Member, IEEE), HAO SHENG[2], LIANYING LIAO[1], CHENGWU LIU[1], AND YEPING XIONG[3]**

[1]College of Automotive Engineering, Changzhou Institute of Technology, Changzhou 213032, China
[2]College of Electrical and Information Engineering, Hunan University of Technology, Zhuzhou 412007, China
[3]Faculty of Engineering and Physical Sciences, University of Southampton, SO16 7QF Southampton, U.K.

Corresponding author: Zhongsheng Chen (chenzs@czu.cn)

This work was supported in part by the National Natural Science Foundation of China under Grant 51975206, in part by the Major Natural Science Foundations of the Higher Education Institutions of Jiangsu Province under Grant 22KJA460002 and Grant 22KJA120001, and in part by the Changzhou Science and Technology Support Plan under Grant CE20225062.

**ABSTRACT** Blade tip-timing (BTT) signals are always seriously under sampled, so reconstruction is much needed for vibration analysis. Blade vibration responses are sparse in order domain and classical compressed sensing (CS) algorithms are difficult to reconstruct vibration orders due to lack of prior sparse information under variable speeds. In order to address this issue, this paper introduces deep learning (DL) into BTT vibration reconstruction and proposes an end-to-end deep compressed sensing (DCS) method. Firstly, a multi-coset BTT measurement model is built under variable speeds and the DCS model is derived in order domain, where a specific convolutional neural network (CNN) is designed. Next, a Simulink model is built to generate training and testing samples. The simulation results show that the convolution layer with the rectified linear unit (ReLU) layer placed after the batch normalization (BN) layer can improve the reconstruction performance and the proposed method has better reconstruction accuracy and efficiency than classical CS algorithms. Finally, experiments are done and the results demonstrate that blade vibration orders can be recovered accurately by the proposed method, which will provide a novel way of BTT signal analysis.

**INDEX TERMS** Blade tip-timing, deep compressed sensing, multi-coset angular sampling, unknown multi-band vibrations, vibration reconstruction.

## I. INTRODUCTION

High-speed rotating blades are widely used in modern industry, such as compressor blades, turbine blades, fan blades, and so on. In practice, different faults or damages of rotating blades are prone to happen due to severe operation conditions including strong vibrations, large centrifugal forces and thermal stresses. It has been reported that more than 70% of blade faults are induced by vibrations [1], [2]. Thus on-line blade vibration monitoring is very important to ensure safety and operational reliability. Traditionally, contact methods were widely studied to monitor blade vibrations. Krause and Ostermann [3] proposed a damage detection algorithm for wind turbine blades based on airborne sounds. Abouhnik and Albarbar [4] proposed a novel health index called empirically decomposed feature intensity level for blade condition assessment. Spitas et al. [5] studied a three-point electrical potential difference method for in-situ monitoring of crack propagating. In addition, strain gauges were also used to measure blade vibrations [6], [7]. However, contact methods have disadvantages of contaminated signals, unexpected intrusion and high cost. As an advanced non-contact method, nowadays blade tip-timing (BTT) has been investigated widely [8], whose advantages include all-blade measurement, no intrusion and long-term service ability. Chen et al. [9] gave a comprehensive review on BTT-based health monitoring.

The associate editor coordinating the review of this manuscript and approving it for publication was Wei Wang.

This work is licensed under a Creative Commons Attribution-NonCommercial-NoDerivatives 4.0 License.
For more information, see https://creativecommons.org/licenses/by-nc-nd/4.0/

However, the intrinsic defect of the BTT method is that vibration signals are seriously sub-sampled [9]. In this case, it is very necessary to reconstruct blade vibrations.

Current challenges of BTT vibration reconstruction can be summarized as three aspects. The first one arises from variable operation conditions due to different mission profiles, which can complicate BTT vibration measurement. The second one is from multi-band vibrations due to system nonlinearity, complex excitations or incipient damages. Accurate multi-band vibration reconstruction is still a difficult task. The third one is lack of prior information of multi-band vibrations. In early studies, blade vibration response is assumed to be a band-pass signal. Under this assumption, Salhi et al. [10] first proposed a method to reconstruct a continuous BTT signal. Chen et al. [11], [12] proposed to reconstruct sub-sampled blade vibrations by using the Shannon sampling theorem and wavelet packet transform. Later, Chen et al. further presented two reconstruction methods under speed fluctuations [13] and variable speeds [14], respectively. Lin et al. [15] presented a novel reconstruction method for non-uniformly sub-sampled BTT data based on the periodically non-uniform sampling theorem. But the assumption of band-pass signals is impractical. Therefore, new reconstruction methods are desirable to overcome the above three challenges.

Blade vibration responses tend to be multi-band [16], which are generally sparse in frequency or order domain. The sparsity opens up new directions of signal reconstruction. Compressed sensing (CS) was first proposed by Donoho et al. [17], which took fully advantages of signal sparsity to recover certain features from sub-sampled signals. Therefore, it is very promising to introduce the CS theorem to reconstruct BTT signals. Chen et al. [18], [19] first built a CS model of BTT measurements. Pan et al. [20] proposed a dictionary learning method for representing BTT signals and then reconstructed blade vibrations by using the basis pursuit algorithm. Spada et al. [21] evaluated several conditions of CS for BTT signals. For the CS model, several classical algorithms have been studied to obtain its unique and stable sparse solution, such as Orthogonal Matching Pursuit (OMP), Multiple Signal Classification (MUSIC), Modified Focal Underdetermined System Solver (MFOCUSS) and Basis Pursuit Denoising (BPDN). Chen et al. [19] compared the performances of the above four reconstruction algorithms in BTT vibration reconstruction. However, most of these algorithms still depend on prior sparse information of original signals [22]. To sum up, unknown multi-band vibration reconstruction is still an obstacle of BTT-based vibration monitoring.

In recent years, deep learning (DL) has achieved great success in many fields due to excellent learning ability, such as image processing [23], speech recognition [24], and so on. Its most advantage is to learn the structure of a signal and obtain effective inherent information, instead of using prior knowledge. In recent years, DL has being combined with CS for image reconstruction. Zisselman et al. [25] presented a

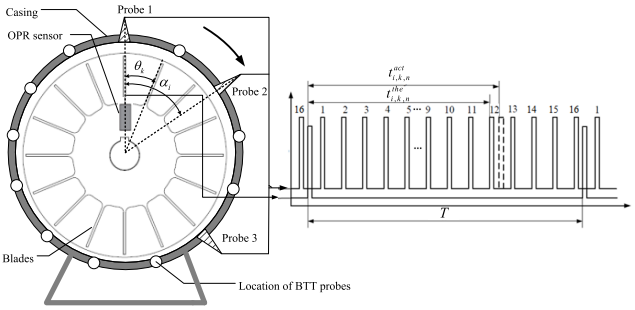


**FIGURE 1.** Schematic diagram of the BTT method.

mathematical framework of compressed learning and then introduced a deep neural network (DNN) for image classification. Ye and Han [26] proposed a general deep learning framework called deep convolutional framelets for image reconstruction.

Inspired by these studies, this paper will introduce DL into BTT vibration reconstruction and propose an end-to-end deep compressed sensing (DCS) method. To the best knowledge of the authors, it is the first to introduce the DL method for multi-band blade vibration reconstruction using sub-sampled BTT signals. The remainder of this paper is organized as follows: In Section II, basic principles of BTT measurement is introduced briefly and then the character of under-sampling is emphasized. In Section III, the CS model of BTT measurements is built in angular domain. Then the DCS-based BTT vibration reconstruction algorithm is described in Section IV. Numerical simulations and experiments are done to validate the proposed method in Section V and Section VI, respectively. In the end, some conclusions are marked in Section VII.

## II. PROBLEM STATEMENT

Basic principle of BTT method can be schematically shown in Figure 1. A blisk is composed of $K$ blades and $I$ BTT probes are mounted in a stationary case around the blisk. A once-per-revolution (OPR) sensor are placed close to the rotating shaft on which one speed mark is made, so timing reference signals can be generated. It is assumed that the OPR sensor is on the same radius as the first BTT probe and the OPR marker is on the same radius as the first blade. Then the angular positions of the $i^{th}(1 \le i \le I)$ BTT probe and the $k^{th}(1 \le k \le K)$ blade relative to the OPR mark are denoted as $\alpha_i$ and $\theta_k$, respectively.

The basis of BTT method is to measure times of arrival (TOAs) when each blade passes each BTT probe [9]. When there are vibrations, the blades will pass BTT probes earlier or later than theoretical TOAs. Therefore, actual TOAs will deviate from theoretical ones, which will lead to time differences. Furthermore, these time differences are strongly related to vibration frequency and amplitude of the blade, so that they can be used to calculate vibration displacements. TOAs of each blade can be collected during

rotation, so the BTT method can measure all-blade vibrations simultaneously.

For the sake of easy understanding, let the blisk rotate clockwise at a constant rotating frequency ($f_r$). When no vibrations, theoretical TOAs of the $k$th blade passing the $i$th BTT probe can be calculated as,

$$t_{i,k,n}^{the} = \begin{cases} [2\pi\ (n-1) + \alpha_i - \theta_k]/2\pi f_r, & \theta_k \leqslant \alpha_i \\ [2\pi n + \alpha_i - \theta_k]/2\pi f_r, & \theta_k > \alpha_i \end{cases} \tag{1}$$

where $n$ denotes the $n$th revolution.

The actual TOAs are denoted as $t_{i,k,n}^{act}$ and then vibration displacement of the $k$th blade measured by the $i$th BTT probe can be calculated as,

$$d_{i,k}[n] = 2\pi f_r R(t_{i,k,n}^{act} - t_{i,k,n}^{the}) \tag{2}$$

where $R$ is the rotating radius of the blade tip.

The main concern in Equations (1) and (2) is about the rotating speed. Under variable rotating speeds, theoretical TOAs are difficult to be calculated accurately. In addition, the sampling time interval is not a constant even though BTT probes are mounted uniformly. It is coincident that BTT probes are mounted circumferentially, so that BTT sampling is a natural angular-domain sampling process. As we all know that angular-domain sampling has always been applied to deal with variable speeds [27]. Thus this paper will perform BTT measurements in angular domain.

In angular domain, theoretical angles of arrival (AOAs) of the $k$th blade passing the $i$th BTT probe under no vibrations can be represented as,

$$\theta_{i,k,n}^{the} = \begin{cases} 2\pi\ (n-1) + \alpha_i - \theta_k, (n = 1, 2, \cdots), & \theta_k \leqslant \alpha_i \\ 2\pi\ (n-1) + 2\pi + \alpha_i - \theta_k, (n = 1, 2, \cdots), & \theta_k > \alpha_i \end{cases} \tag{3}$$

In order to illustrate the principle clearly, the rotating speed during each revolution is assumed to be constant. Then actual AOAs of the $k$th blade passing the $i$th BTT probe can be calculated as,

$$\begin{aligned} \theta_{i,k,n}^{act} &= 2\pi\ (n-1) + 2\pi f_n \left( t_{i,k,n}^{act} - \sum_{p=1}^{n-1} T_p \right) \\ &= 2\pi\ (n-1) + \omega_n \Delta t_n^{ik} \end{aligned} \tag{4}$$

where $T_p, f_n$ are the period of the $p$th revolution and the frequency of the $n$th revolution, respectively, $\omega_n = 2\pi f_n$ and $\Delta t_n^{ik}$ is the measured passing time of the $k$th blade passing the $i$th BTT probe in the $n$th revolution.

Combining Equation (3) with Equation (4), angular-domain sampled vibration displacements of the $k$th blade measured by the $i$th BTT probe can be calculated as,

$$y_{i,k}\ [n] = \left( \theta_{i,k,n}^{act} - \theta_{i,k,n}^{the} \right) R \tag{5}$$

Based on Equations (3)∼(5), one can see that angular-domain vibration displacements are strongly related to the rotating angular speed in the $n$th revolution. In engineering applications, $\omega_n$ in Equation (4) is often defined as $\omega_n = 2\pi \big/ (t_n - t_{n-1})$ in order to reduce the angular bias. Here $t_n$, $t_{n-1}$ are the ending times of the $n$th and ($n$-1)th revolutions, respectively. However, $\omega_n$ cannot be looked as a constant if the rotating angular speed changes rapidly. In this case, calibration methods need to be explored, which are out of the scope of this paper. In particular, Equations (3)∼(5) still hold under constant rotating speeds.

As stated in previous works [14], [15], BTT signals are seriously sub-sampled and it is difficult to directly obtain 'true' blade vibration characteristics due to alias. Thus how to reconstruct BTT vibrations under variable rotating speeds is an urgent problem to be solved.

## III. COMPRESSED SENSING MODEL OF BTT VIBRATIONS IN ANGULAR DOMAIN

True vibration displacement of the $k$th blade in angular domain is assumed to be $y(\theta)$. According to Figure 1, $y(\theta)$ is sampled for $I$ times during each revolution. Furthermore, such a sampling scheme can be equivalent to a multi-coset angular sampling (MCAS) process [19]. According to its principle, the multi-coset sampling is a selection of certain samples from the uniform sampling at the Nyquist rate. Here the multi-coset period is denoted as $L$ and $L$ virtual BTT probes are uniformly mounted. The number of each probe is denoted from 1 to $L$ clockwise. Then practical BTT probes are considered to be selected from these $L$ virtual BTT probes, which can be uniformly or non-uniformly mounted. Here $L$ satisfies $L \geq 2E_o^{\max}$ due to the Nyquist sampling rate, where $E_o^{\max}$ is the maximum vibration Engine Order (EO) of the blade.

The Nyquist-sampled vibration signals can be written as,

$$y\,[n] = y\,(n\Delta\theta)\,, \quad \Delta\theta = 2\pi \big/ L \tag{6}$$

Then $I$ actual BTT probes are chosen from the above $L$ virtual BTT probes and a MCAS pattern of $(L, I, C)$ is formed. Here $C = \{c_i : 1 \leq i \leq I\}$ and $c_i$ is the number of the $i$th probe ($0 \leq c_1 < c_2 \cdots < c_I \leq L-1$). In this way, sampled vibrations of the $i$th BTT probe can be represented as,

$$\bar{y}_i\,[n] = y\,[nL + c_i]\,, \quad i = 1, \ldots, I \tag{7}$$

where the sampling interval is denoted as $\Delta\theta_I = L\Delta\theta$.

In practice, $I$ is always much less than $L$ due to the limitations of space and cost, so that $\bar{y}_i\,[n]$ is always sub-sampled. It should be pointed out that $y\,[n]$ can be used to perfectly recover true EOs of the blade. Thus the remaining problem is how to correctly reconstruct $y\,[n]$ based on $\bar{y}_i\,[n]$.

For multi-band blade vibrations, they are also sparse in order domain. Thus it is probable to reconstruct $y\,[n]$ from sub-sampled signals ($\bar{y}_i\,[n]$) by using the CS theorem. Firstly, the relation between $y\,[n]$ and $\bar{y}_i\,[n]$ in order domain can be

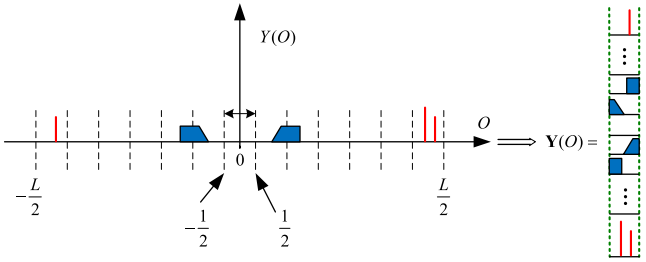


**FIGURE 2.** The sub-band division of $Y(O)$.

built as follows [15].

$$\bar{Y}_i(O) = \frac{e^{j2\pi Oc_i}}{L} \sum_{k=1}^{L} e^{-j\frac{2\pi}{L}\left(k-\frac{L+1}{2}\right)c_i} \times Y\left(O - \left(k - \frac{L+1}{2}\right)\right) \tag{8}$$

where $O$ denotes the order ($O \in [-1/2, 1/2]$) and $\bar{Y}_i(O)$, $Y(O)$ are the discrete Fourier transforms of $\bar{y}_i[n]$, $y[n]$, respectively.

Furthermore, physical meaning of Equation (8) can be described based on Figure 2, where the entire order band ($Y(O)$) is equally divided into $L$ sub-bands and the $l$th sub-band is represented as follows.

$$Y_l(O) = Y\left(O - \left(l - (L+1)/2\right)\right), \quad l = 1, 2, \cdots L \tag{9}$$

According to Equations (8) and (9), $\bar{Y}_i(O)$ can be looked as the weighed sum of sub-bands of $Y(O)$. In this case, for $I$ BTT probes, Equation (8) can be expressed as the following matrix form.

$$\bar{Y}(O) = \Phi Y(O) \tag{10}$$

where, $\bar{Y}(O) = [\bar{Y}_1(O)\exp(-j2\pi Oc_1), \cdots \bar{Y}_I(O)\exp(-j2\pi Oc_I)]^T$, $Y(O) = [Y_1(O), \cdots Y_L(O)]^T$, as shown in the equation at the bottom of the next page.

In Equation (10), $\bar{Y}(O) \in R^{I\times nfft}$ is the measurement matrix which can be calculated by $I$ actual BTT signals. $\Phi \in R^{I\times L}$ is the sensing matrix. $Y(O) \in R^{L\times nfft}$ is the sub-band matrix which is formed based on $Y(O)$. Here $nfft$ denotes the point number of Fourier transform of $\bar{y}_i[n]$. Based on Figure 2, $Y(O)$ only has few non-zero rows, so it is sparse in order domain. Moreover, $I < L$. Thus Equation (10) can be looked as a CS model of unknown $Y(O)$. Furthermore, the sparsity basis is the Fourier basis function.

Next, the reconstruction task is transformed to find the unknown$Y(O)$ based on the known $\bar{Y}(O)$ and $\Phi$. According the CS theorem, the solution of Equation (10) can be represented as the following P0 problem.

$$P0: \ \min ||Y(O)||_0 \quad s.t. \bar{Y}(O) = \Phi Y(O) \tag{11}$$

where $\|\cdot\|_0$ is the $\ell_0$-norm operator.

## IV. DEEP COMPRESSED SENSING-BASED BTT VIBRATION RECONSTRUCTION

### A. BASIC FRAMEWORK

Classical OMP, MUSIC, BPDN and MFOCUSS algorithms have been used to solve the P0 problem, as shown in Equation (11). However, these classical CS algorithms are seriously limited by the restriction of Restricted Isometry Property (RIP) [28] and slow optimization process. In order to overcome this limitation, an end-to-end DCS framework is proposed in Figure 3, which is composed of five parts: measurement of TOAs, calculation of AOAs, multi-coset measurement model, CS model and DNN. Furthermore, there are four key operations: angular sampling, multi-coset sampling, compressed sensing and learning sensing. Key advantages of this framework include: i) Variable conditions can be handled by transferring time domain to angular domain. ii) CS of unknown multi-band vibrations can be obtained by introducing multi-coset sampling. iii) High-fidelity and fast reconstruction can be achieved by using DL algorithms.

Next, the flowchart of DNN-based reconstruction is shown in Figure 4. The model inputs are $\bar{Y}(O)$ and $\Phi$, both of which are obtained from the $I$ BTT probes. Firstly, signal preprocessing of $\bar{Y}(O)$ is done. The pseudo-reconstruction signal of $Y(O)$ is calculated as follows.

$$\widetilde{Y}(O) = \left(\Phi^H \Phi\right)^{-1} \Phi^H \bar{Y}(O) \tag{12}$$

where $\Phi^H$ is the transpose of $\Phi$.

However, $\widetilde{Y}(O)$ is a complex signal, so it cannot be directly input to the DNN model. In order to deal with it, the real and imaginary parts of $\widetilde{Y}(O)$ are concatenated to form a higher-dimension matrix $\tilde{Y}_{con}(O)$.

$$\tilde{Y}_{con}(O) = \left[Re\left(\widetilde{Y}(O)\right), Im\left(\widetilde{Y}(O)\right)\right] \tag{13}$$

Furthermore, $\tilde{Y}_{con}(O)$ is normalized to accelerate the training convergence. By this way, each element of $\tilde{Y}_{con}(O)$ is normalized between [1, 0].

$$\widetilde{Y}_{Norm}(O) = \mathrm{Norm}(\widetilde{Y}_{Con}(O)) \tag{14}$$

The output of the DNN model is an $L$-dimension vector $\hat{S}$ denoting band occupancy status, whose element ($\hat{S}_i$) is equal to 0 or 1. That is to say,

$$\hat{S}_i = \begin{cases} 0, & if\ vacant\ band \\ 1, & if\ non-vacant\ band \end{cases} \tag{15}$$

After training, the DNN model is well built. At the testing stage, $\hat{S}$ will be calculated by each testing sample and new sensing matrix $\Phi_{new}$ is formed by retaining the columns of $\Phi$ with indices corresponding to $\hat{S}_i$=1. Then $Y(O)$ can be reconstructed as follows.

$$\hat{Y}(O) = \Phi_{new}^{\dagger} \bar{Y}(O) \tag{16}$$

where $\Phi_{new}^{\dagger}$ is the pseudo inverse of $\Phi_{new}$.

In the end, the target $Y(O)$ can be obtained by re-arranging $\hat{Y}(O)$, so true blade vibration characteristics can be recovered.

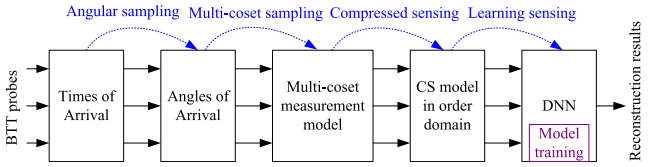


**FIGURE 3.** The proposed DCS framework for BTT signal reconstruction.

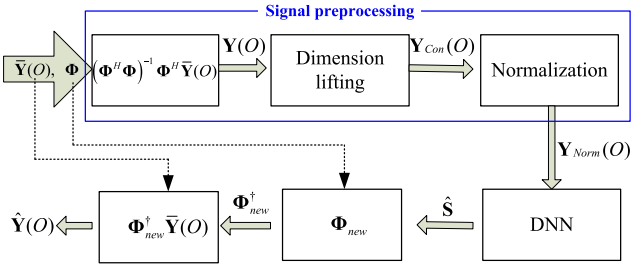


**FIGURE 4.** Flowchart of DNN-based reconstruction.

### B. DESIGN OF A SPECIFIC CNN MODEL

#### 1) MODEL ARCHITECTURE

The key of Figure 4 is how to design a proper DNN model. As we all know that CNN has many advantages such as simple structure, less training parameters and adaptability. But by now, there have been no standard rules of selecting the CNN architecture. In this paper, a CNN with 4 convolutional layers is selected by hand. Next this paper proposes to design a specific CNN model as shown in Figure 5, which is composed of one input layer, four convolution layers, one pooling layer, two fully connected layers and one output layer.

For the above CNN model, the rectified linear unit (ReLU) activation function and the Max pooling are used. Traditionally, a Batch Normalization (BN) layer is always placed before the activation function to reduce internal covariate shift and accelerate training [29]. Recently, some studies shown that the BN layer could be placed before the ReLU layer to update the weights in a suboptimal way [30]. In addition, Hinton et al [31] first proposed to use 'Dropout' to reduce overfitting on a small training set. Later, Park and Kwak [32] analyzed the effect of Dropout in convolution layers. In this case, both a BN layer and a Dropout layer are also introduced to build the convolution layer. Differently, the BN and Dropout layers are combined together and then placed after the ReLU layer. A small dropout probability is applied for the Dropout layer.

#### 2) MODEL PARAMETERS

There has been no theoretical heuristics of determining optimal hyperparameters of a DNN. Here, the hyperparameters of the above CNN model are obtained by many trials. In order to evaluate the reconstruction performance of a CNN model, a metric of reconstruction accuracy is defined as follows.

$$R_a = \frac{\text{number of correct reconstructions}}{\text{number of test samples}} \tag{17}$$

Furthermore, if the reconstructed vector $(\hat{S})$ of a testing sample is the same as the label vector, it is called as 'a correct reconstruction'. Based on Equation (17), some architecture parameters of the extended CNN model are obtained and listed in Table 1, including the filter size and the filter number of each layer. The input layer is a $I \times L \times 2$ matrix corresponding to $\tilde{Y}_{con}(O)$. The kernel sizes of the four convolution layers are $1 \times 150$, $1 \times 50$, $1 \times 20$ and $1 \times 10$, which is denoted as {150-50-20-10}. The kernel size of the Max pooling layer is $2 \times 2$. The neuron numbers of the first and second fully connected layers are 1024 and 128, respectively. The output is a $L \times 1$ vector corresponding to the vector $(\hat{S})$ of band occupancy status. These parameters can be iteratively updated during training. After being trained, the CNN model is used to infer the band occupancy status of unknown multi-band BTT vibration signals. Once $\hat{S}$ is obtained, $Y(O)$ can be reconstructed based on Equation (16).

## V. NUMERICAL SIMULATIONS

### A. SIMULINK-BASED BTT SIGNAL SIMULATION

In order to validate the proposed DCS method, numerical simulations are done to generate BTT training and testing datasets. For a real complex-profile blade, its mode shapes are often complicated. In order to generate easily multi-band tip-timing signals, a straight blade is considered and its main mode is the first-order bending mode. Under the simplified assumption, dynamic behavior of the blade can be represented by a single-degree-of-freedom (SDOF) lumped-parameter model and its vibration equation is written as follows [33].

$$m_{eq}\ddot{y}(t) + c_{eq}\dot{y}(t) + k_{eq}y(t) = F(t) \tag{18}$$

where $m_{eq}, c_{eq}, k_{eq}$ are the equivalent mass, damping and stiffness, respectively. $y(t)$ denotes blade vibration displacement. $F(t)$ denotes the vibration excitation.

$$\Phi = \frac{1}{L} \times \begin{bmatrix} \exp\left(-j2\pi c_1\left(1-(L+1)/2\right)/L\right) & \cdots & \exp\left(-j2\pi c_1\left(l-(L+1)/2\right)/L\right) & \cdots & \exp\left(-j2\pi c_1\left(L-(L+1)/2\right)/L\right) \\ \vdots & & \vdots & & \vdots \\ \exp\left(-j2\pi c_i\left(1-(L+1)/2\right)/L\right) & \cdots & \exp\left(-j2\pi c_i\left(l-(L+1)/2\right)/L\right) & \cdots & \exp\left(-j2\pi c_i\left(L-(L+1)/2\right)/L\right) \\ \vdots & & \vdots & & \vdots \\ \exp\left(-j2\pi c_I\left(1-(L+1)/2\right)/L\right) & \cdots & \exp\left(-j2\pi c_I\left(l-(L+1)/2\right)/L\right) & \cdots & \exp\left(-j2\pi c_I\left(L-(L+1)/2\right)/L\right) \end{bmatrix}$$

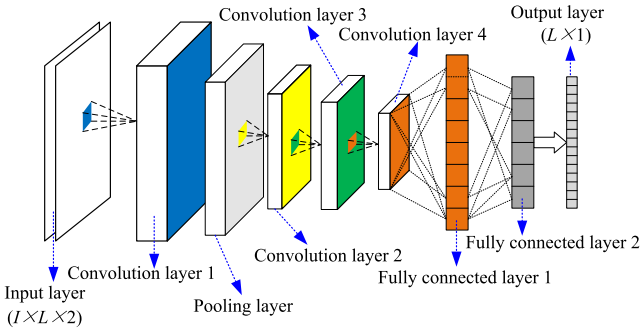


**FIGURE 5.** Basic architecture of the specific CNN model.

**TABLE 1.** Architecture parameters of the specific CNN model.

| Layer | Filter size | Number of filters | Output dimension |
|---|---|---|---|
| Input layer | / | / | $I\times L\times 2$ |
| Convolution layer 1 | $1\times 100$ | 128 | $I\times L\times 128$ |
| Max pooling layer | $2\times 2$ | / | / |
| Convolution layer 2 | $1\times 50$ | 64 | $I\times L\times 64$ |
| Convolution layer 3 | $1\times 20$ | 32 | $I\times L\times 32$ |
| Convolution layer 4 | $1\times 10$ | 16 | $I\times L\times 16$ |
| Fully connected layer 1 | / | / | $1024\times 1$ |
| Fully connected layer 2 | / | / | $128\times 1$ |
| Output layer | / | / | $L\times 1$ |

As for variable conditions, it is easy to realize linearly variable speeds, so the rotating frequency ($f_r(t)$) is assumed to increase linearly in this paper. That is to say,

$$f_r(t) = f_0 + (f_e - f_0)\, t / T_s \tag{19}$$

where $f_0, f_e$ are the rotating frequencies at the starting time and the ending time, respectively. $T_s$ is the total simulation time. Furthermore, three synchronous excitations are chosen to simulate multi-band blade vibrations. That is to say, the vibration excitation can be written as,

$$F(t) = \sum_{i=1}^{3} A_i \sin\left(2\pi EO_i f_r\,(t)\, t + \varphi_i\,(t)\right) \tag{20}$$

where $EO_i\,(i = 1, \ldots, 3)$ denoted the $i$th EO and $A_i$, $\varphi_i\,(t)$ are the corresponding amplitudes and phases.

Next the BTT sampling process in angular domain is simulated in Matlab/Simulink environment [34] and the whole model is shown in Figure 6(a), which is composed of the system model and angular-domain sampling process. Firstly, the SDOF model in Equation (18) is built as Figure 6(b). Then the angular-domain sampling process of thirteen BTT probes is built by using the 'Hit Crossing' Block and the 'Switch' Block. The details of the 'Sensor set 1' is shown in Figure 6(c), which is the same as those of 'Sensor set 2' and 'Sensor set 3'. The key is to determine angular-sampling times. For each rotating blade, its angular position is calculated as $\theta\,(t) = \theta_0 + 2\pi f_r\,(t)\, t$. When the blade tip passes the $i$th BTT probe, the angular sampling time in the $n$th revolution should satisfy the following condition,

$$2\pi f_r\,(t)\, t = \alpha_i - \theta_0 + 2\pi n \tag{21}$$

According to the BTT principle, each angular-sampling time can be calculated by $\sin\left(2\pi f_r\,(t)\, t\right) = \sin\left(\alpha_i - \theta_0\right)$, where the left part is carried out by using the 'Chirp Signal' Block and the right part is set as the threshold of the 'Hit Crossing' Block.

**TABLE 2.** Parameter values in the simulink model.

| Parameters | Values |
|---|---|
| $\{m_{eq}, c_{eq}, k_{eq}\}$ | $\{0.1\,\text{kg}, 10\,\text{N}\cdot\text{s/m}, 4\times10^5\,\text{N/m}\}$ |
| $\{f_0, f_e\}$ | {50 Hz, 200 Hz} |
| $T_s$ | 50 seconds |
| $\{A_1, A_2, A_3\}$ | {4, 3, 2} |
| $\{EO_1, EO_2, EO_3\}$ | {1, 2, 5} |
| $\{\varphi_1(t), \varphi_2(t), \varphi_3(t)\}$ | {0, 0, 0} |
| $L$ | 13 |
| $\{\alpha_1\text{-}\theta_0, \alpha_2\text{-}\theta_0, \text{K}, \alpha_{13}\text{-}\theta_0\}$ | $\{\pi/13, 3\pi/13, \text{K}, 25\pi/13\}$ |
| Learning rate ($\eta$) | 0.001 |
| Optimizer | Adam[35] |

Parameter values in the Simulink model are selected artificially and listed in Table 2. Then angularly-sampled blade vibration displacements by each BTT probe can be obtained. Firstly, angular-domain vibration signal sampled by the thirteen BTT probes is shown in Figure 7(a) and its order power spectrum is plotted in Figure 7(b). The Nyquist sampling theorem is satisfied when $L = 13$, so the three EOs can be captured accurately.

Next it needs to generate training and testing samples to evaluate the DCS model. Here $L = 13$, $I = 4$ and $C$ is generated randomly for each sample. For each MCAS pattern of $(L, I, C)$, angular-domain samples $(\bar{y} = (\bar{y}_1[n], \ldots, \bar{y}_I[n]))$ are obtained by adding stochastic Gaussian noises with different signal-to-noise ratios (SNRs) and the corresponding band occupancy status vector $(\hat{S})$ is labeled. Then each pair of $\left(\bar{y}, \hat{S}\right)$ constitutes a sample and 14000 simulated samples are generated by this way. One half is used for training and the other half is used for testing (e.g. both equal to 7000). After many trials, the Adam algorithm is used as the optimizer and the learning rate is equal to 0.001.

### B. EFFECTS OF THE SPECIFIC CNN ARCHITECTURE

The effects of the CNN architecture on the reconstruction accuracy need to be investigated. Firstly, Four CNNs with different kernel sizes (i.e. {10-5-5-5}, {50-25-25-25}, {100-50-20-10} and {150-50-20-10}) are studied under different SNRs, and the corresponding reconstruction

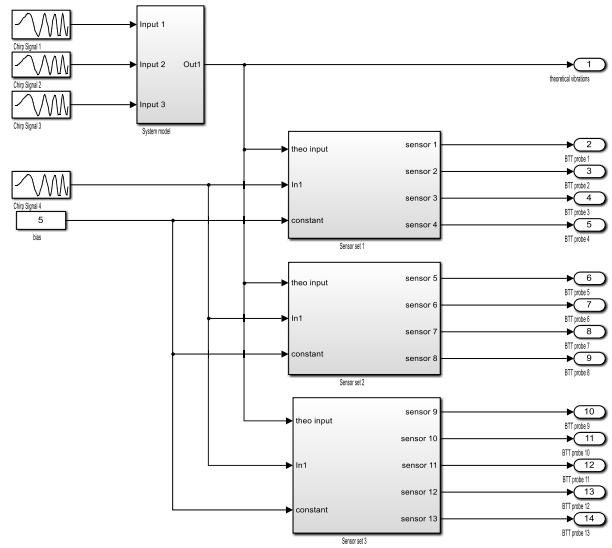


(a) The whole simulation model

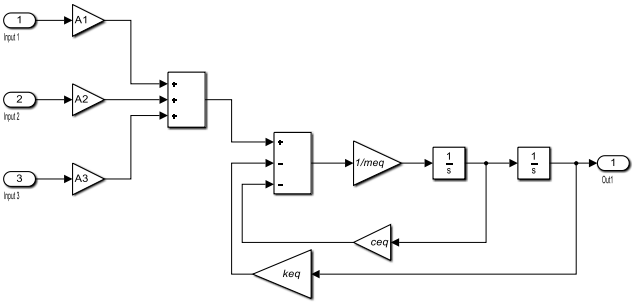


(b) Details of the 'System model' module

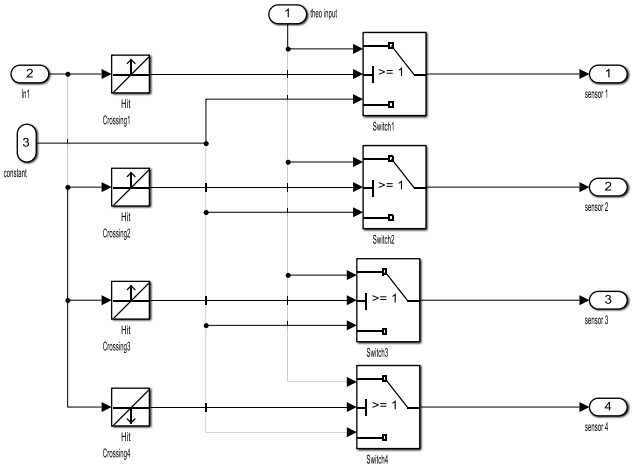


(c) Details of the 'Sensor set 1' module

**FIGURE 6.** Simulink model of BTT sampling process in angular domain.

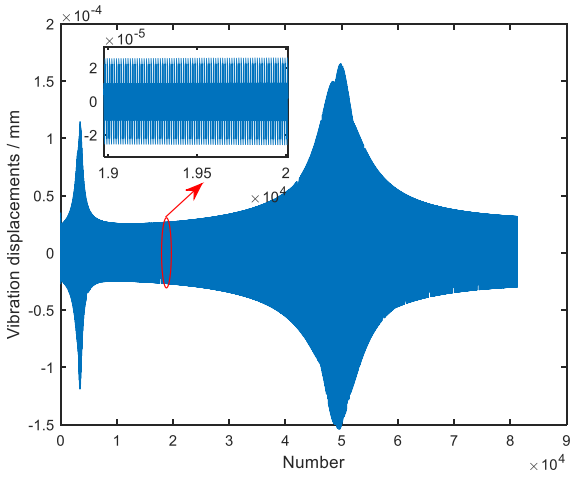


(a) Angular-domain signal

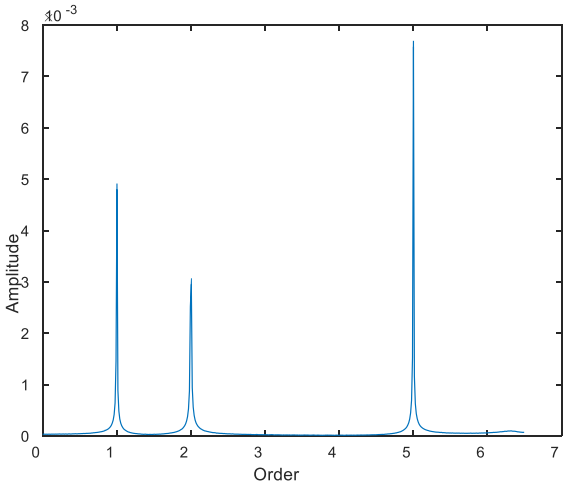


(b) Order power spectrum

**FIGURE 7.** Sampled vibration displacements by thirteen BTT probes.

accuracies are compared in Figure 8(a). It can be seen that: i) The reconstruction accuracy increases with the SNR, ii) Filters with a larger width perform better than those with a smaller width, iii) Among the four kernel sizes, {100-50-20-10} leads to the best reconstruction accuracy.

Next, two kinds of convolutional layers (i.e. the ReLU layer placed before and after the BN layer) are compared in Figure 8(b). One can see that the former has better reconstruction performance. In addition, other architecture parameters may also affect the reconstruction accuracy, which belongs to another and open research scheme. Thus it will not be discussed in this paper.

### C. COMPARISONS WITH CLASSICAL RECONSTRUCTION ALGORITHMS

In the previous work [15], OMP, MUSIC, BPDN and MFOCUSS algorithms have been studied to reconstruct BTT vibrations under variable speeds. Here the proposed method will be compared with both these four CS algorithms and the SPGL1 algorithm [36]. The simulation results are shown in Figure 9. One can see that the reconstruction accuracy value of the proposed method is much larger than those of the five algorithms under different SNRs. Also the reconstruction accuracy can be further improved if more training samples are used. The SPGL1 algorithm performs more accurately than

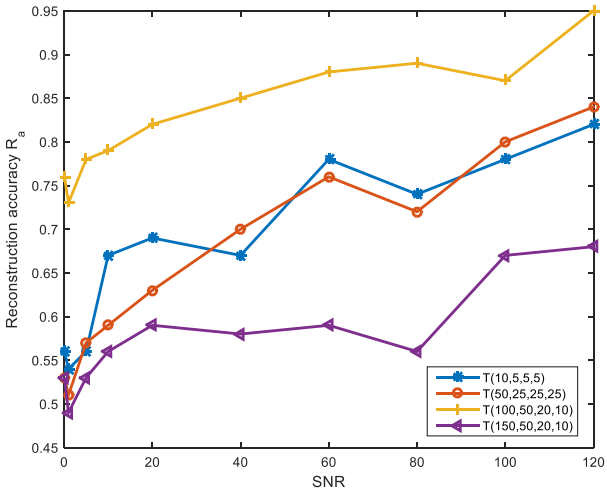


(a) Different filter sizes

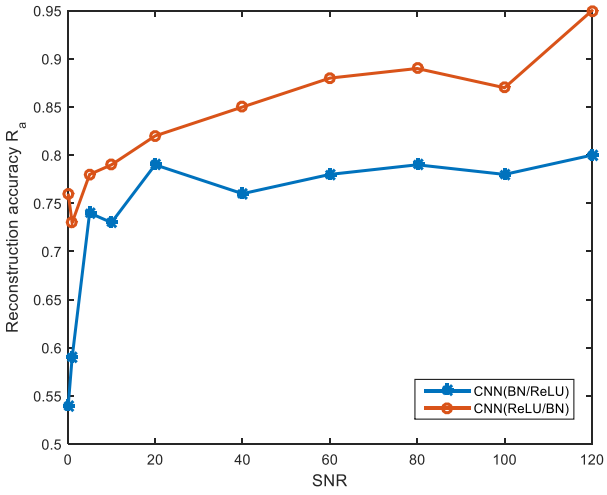


(b) Different convolution layers

**FIGURE 8.** Reconstruction accuracies under different CNN architectures.

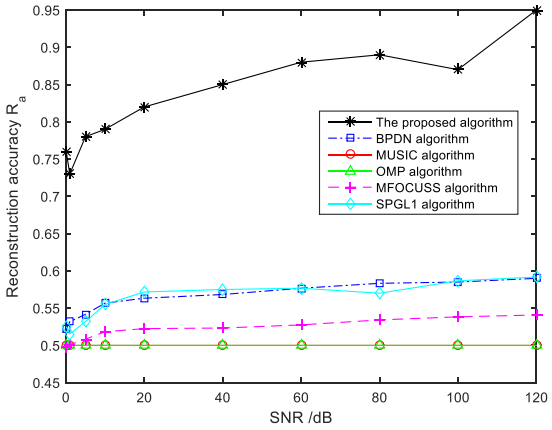


**FIGURE 9.** Comparison of the proposed method with classical CS algorithms.

**TABLE 3.** Key experimental parameters.

| Parameters | Values |
|---|---|
| Blade material | 40 Cr steel |
| Blade length | 34 mm |
| Blade width | 11 mm |
| Blade tip thickness | 3 mm |
| Blade tip radius | 69 mm |
| Number of blades | 32 |
| Number of BTT probes | 4 |
| Number of OPR sensors | 1 |
| Angle of adjacent BTT probes | 6° |
| Variable rotating speed | 5000~11400 rpm |
| Acceleration time | 200 seconds |

the four CS algorithms. In addition, the calculation time of the DCS model on the entire testing set is only about 50 seconds yet the corresponding time of standard CS algorithms is about 215 seconds. Hence the proposed method also has much higher reconstruction speed.

## VI. EXPERIMENTAL VALIDATIONS

### A. EXPERIMENTAL SET-UP AND DATASETS

To further validate the proposed DCS method, an experimental set-up of BTT-based vibration measurement of rotating blades is built as shown in Figure 10. The whole experimental system is composed of a supporting base, an electrical motor, a testing bladed disk, a magnetic exciter, four BTT probes, a once-per-revolution reference sensor, a protection cover, a data acquisition device and vibration analysis software. The electrical motor was mounted under the supporting base. BTT probes were fixed around the bladed disk through the holes in the protection cover and the angle between two adjacent BTT probes is equal to 6 degrees. The OPR sensor is mounted near the center of the bladed disk. Finally, key experimental parameters are listed in Table 3.

At the beginning of the experiment, the rotating speed increases to 5000rpm. Then the range of variable rotating speed is set as 5000rpm∼11400rpm and the total acceleration time is equal to 200 seconds. Thus the rotating speed is close to increase linearly. During the whole acceleration process, OPR signals and TOAs are collected, which are used to calculate angular-domain vibration displacements. The four BTT probes are numbered 1#, 2#, 3# and 4#. The first blade passing the 1# BTT probe is numbered 'Blade 1'and then other blades are numbered from 'Blade 2' to 'Blade 32' along the direction of rotation. According to installation angles of the four BTT probe, the MCAS pattern is represented as $(60,\ 4,\ \{0,\ 1,\ 2,\ 3\})$. Here Blade 4 is randomly selected as the target blade.

BTT vibration displacements of Blade 4 measured by 1#, 2#, 3# and 4# probe are shown in Figure 11, where all peaks mean that some synchronous resonances happen at those times. For example, there is a peak during 8000∼9000 revolutions and the corresponding speed range is equal to

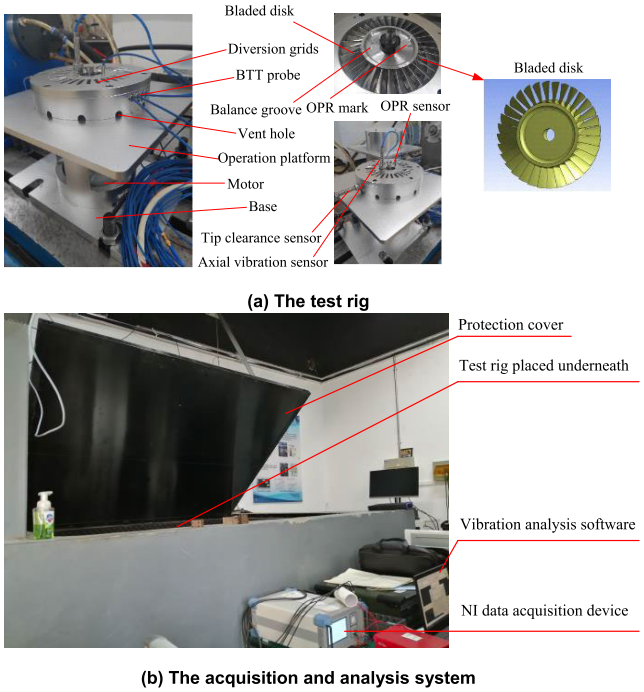


**FIGURE 10.** Experimental set-up.

8000∼8500rpm. Furthermore, vibration EO during 8000∼8500rpm is equal to 15 according to the Campbell diagram of the blade [37]. Therefore, it is obvious that the peak is caused by the 15$^{th}$ EO synchronous vibration. Next measured vibration signal during 8000∼9000 revolutions is used to generate training and testing samples, which is shown in Figure 12. The sampled data is divided into a block with size of 4 × 1000 and the block number is equal to 7000. Then 7000 data blocks are used as the training samples and 3500 data blocks selected randomly are used as the testing samples. It must be pointed out that the reconstructed order band is equal to [−30, 30]. In this case, although there seems only to be an EO (e.g. 15), the sparsity in order domain is equal to 2 (−15 and 15). Therefore, experimental datasets are made from double-band vibration signals.

### B. VALIDATION OF THE PROPOSED DCS METHOD

To validate the DCS method, $\bar{Y}(O)$ is calculated based on measured vibration signals of four actual BTT probes and $\Phi$ is obtained based on the arrangement of four BTT probes, as defined in Equation(10). Next the preprocessing process including Equations (12)∼(14) is carried out to obtain the input of the specific CNN model. According to the MCAS scheme, the whole order band (e.g. [−30, 30]) of blade vibration is equally divided into 60 sub-bands and the dimension of the band occupancy status vector ($\hat{S}$) is equal to 60. Based on these, training and testing datasets can be constructed. Then training samples are used to train the specific CNN model and the number of iterations is equal to 5. Here model architecture parameters listed in Table 1 are utilized according to

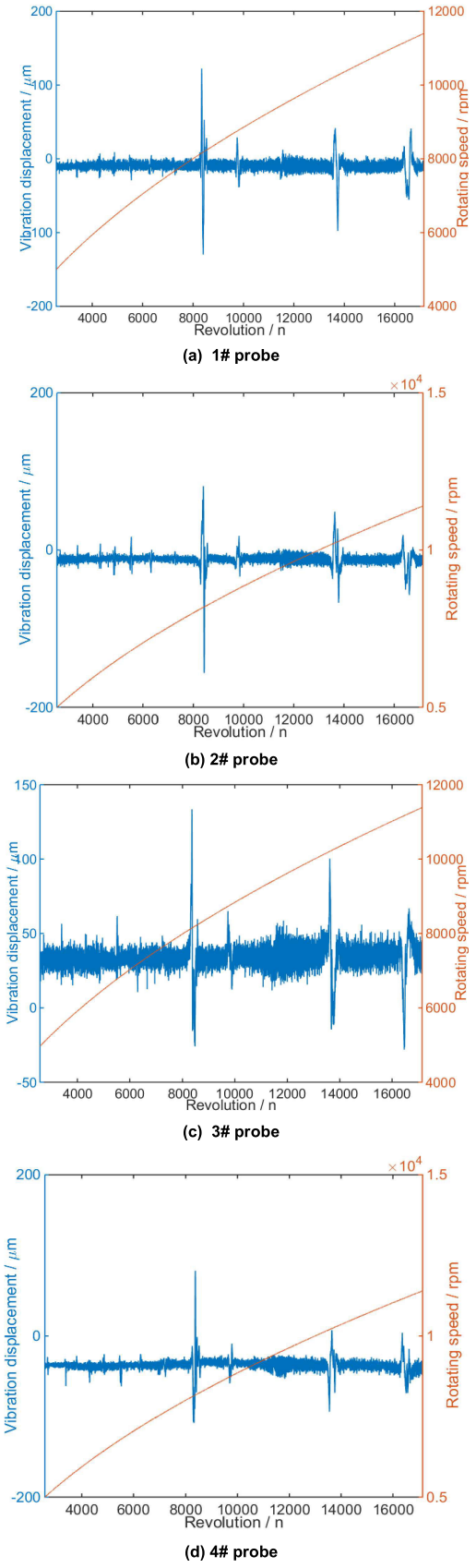


**FIGURE 11.** BTT vibration displacements of Blade 4 by four probes.

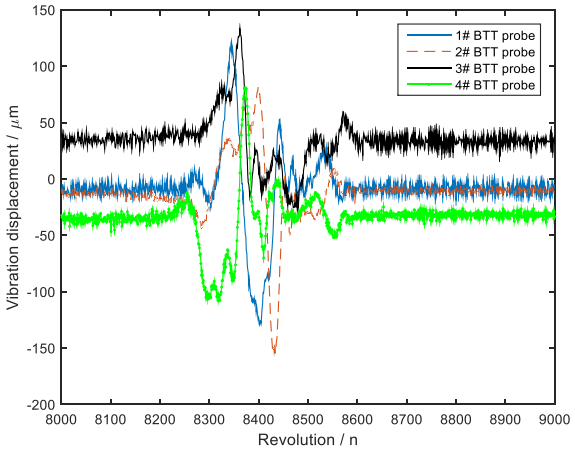


**FIGURE 12.** Vibration signals during 8000∼9000 revolutions.

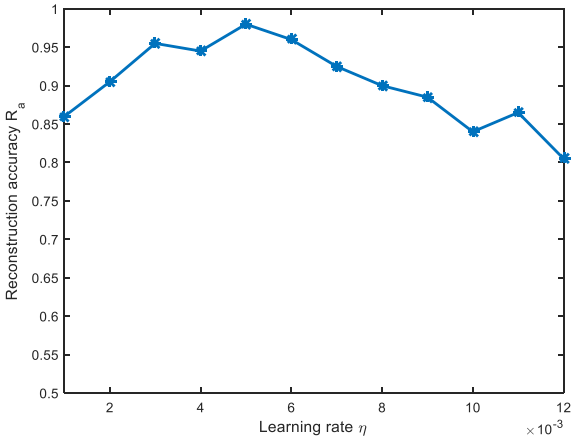


**FIGURE 13.** Effects of the learning rate.

aforementioned simulation results. Finally, testing samples are used to calculate the reconstruction accuracy $R_a$.

The relation between the reconstruction accuracy ($R_a$) and the learning rate ($\eta$) is shown in Figure 13. It can be seen that $R_a$ will reach the maximum value when $\eta \approx 0.005$. Then the trained DCS model with $\eta = 0.005$ is used to recover the order spectra of Blade 4 in testing samples and typical reconstruction result is shown in Figure 14. It should be emphasized that the reconstruction process does not use any prior information of order bands.

It can be seen from Figure 13 and Figure 14 that: 1) The reconstruction accuracy is close to 98% when the learning rate is close 0.005; 2) True vibration EOs can be reconstructed effectively by the proposed DCS-based reconstruction method. Meanwhile, there are small biases which may be caused by manufacturing and measurement errors. In addition, the pre-trained network by simulation signals is used to run inference on experimental data and the results show that the reconstruction accuracy is less than 50%. It means that the generalization ability of the proposed method is not good, which can be explained by the fact that the generalization ability of CNN models is poor.

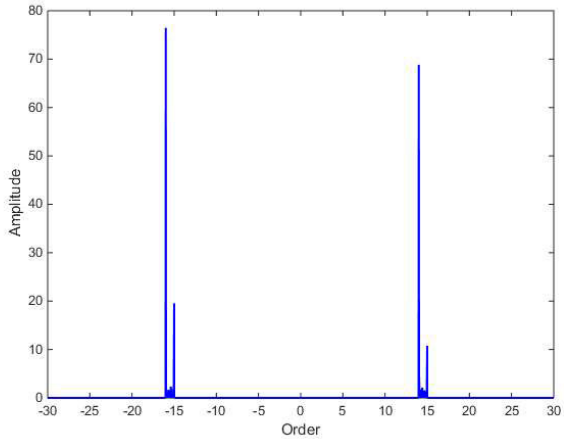


**FIGURE 14.** Reconstruction results of vibration EOs.

## VII. CONCLUSION

In order to accurately and fast reconstruct BTT vibrations under variable rotating speeds, this paper proposes an end-to-end DCS method. The main novelties of the paper include the following three aspects:

(1) An end-to-end DCS-based framework of BTT vibration reconstruction under variable speeds is proposed, including angular sampling, multi-coset sampling, compressed sensing and learning sensing.

(2) A DCS model of BTT measurements under variable speeds is derived in angular domain, where a CNN model is built by using specific convolution layers with the ReLU layer placed after the BN layer.

(3) A DL-driven CS-recovery procedure is introduced to the field of BTT vibration analysis. The proposed DCS method is better than classical reconstruction algorithms from the perspective of reconstruction accuracy and speed.

As for the proposed method, there is still a challenge due to multimode shapes of the bladed disk, which will cause tip-timing signal derivations and reduce the reconstruction performance. It is desirable to build a multi-degree-of-freedom mechanical model and study how to reduce the effects of other mode shapes. Also, poor generalization ability of the proposed method is observed. In future, transfer learning should be a promising direction to address this issue [22], [38]. In addition, other types of DNNs deserve to be further studied for comparison with CNN, such as multilayer perceptron (MLP), ResNet, and so on.

## APPENDIX

## NOMENCLATURE

| | |
|---|---|
| AOAs | Angles of arrival |
| BN | Batch Normalization |
| BPDN | Basis pursuit denoising |
| BTT | Blade tip-timing |
| CNN | Convolutional neural network |
| CS | Compressed sensing |
| DCS | Deep compressed sensing |
| DL | Deep learning |

| | |
|---|---|
| DNN | Deep neural network |
| EO | Engine Order |
| MCAS | Multi-coset angular sampling |
| MFOCUSS | Modified Focal Underdetermined System Solver |
| MUSIC | Multiple signal classification |
| OMP | Orthogonal matching pursuit |
| OPR | Once-per-revolution |
| ReLU | Rectified linear unit |
| RIP | Restricted Isometry Property |
| SDOF | Single-degree-of-freedom |
| SNRs | Signal-to-noise ratios |
| TOAs | Times of arrival |

## ACKNOWLEDGMENT

The authors would thank the experimental set-up provided by the Beijing Key Laboratory of Health Monitoring and Self-Recovery for High-End Mechanical Equipment, Beijing University of Chemical Technology.

## REFERENCES

[1] M. Witos, "High sensitive methods for health monitoring of compressor blades and fatigue detection," *Sci. World J.*, vol. 29, Sep. 2013, Art. no. 218460.

[2] J. W. Lin, J. H. Zhang, G. C. Zhang, G. J. Ni, and F. R. Bi, "Aero-engine blade fatigue analysis based on nonlinear continuum damage model using neural networks," *Chin. J. Mech. Eng.*, vol. 25, pp. 338–345, Feb. 2020.

[3] D. Knappett and J. Garcia, "Blade tip timing and strain gauge correlation on compressor blades," *Proc. Inst. Mech. Eng., G, J. Aerosp. Eng.*, vol. 222, no. 4, pp. 497–506, Jun. 2008.

[4] J. P. Roberts, "Comparison of tip timing with strain gauges for rotor blade vibration measurement," in *Proceedings of Lecture Series on Tip Timing and Tip Clearance Problems in Turbomachines*. Sint-Genesius-Rode, Belgium: Von Karman Institute, 2007.

[5] T. Krause and J. Ostermann, "Damage detection for wind turbine rotor blades using airborne sound," *Struct. Control Health Monit.*, vol. 27, p. e2520, Feb. 2020.

[6] A. Abouhnik and A. Albarbar, "Wind turbine blades condition assessment based on vibration measurements and the level of an empirically decomposed feature," *Energy Convers. Manag.*, vol. 64, pp. 606–613, Dec. 2012.

[7] V. Spitas, C. Spitas, and P. Michelis, "A three-point electrical potential difference method for in situ monitoring of propagating mixed-mode cracks at high temperature," *Measurement*, vol. 43, no. 7, pp. 950–959, Aug. 2010.

[8] S. Heath and M. Imregun, "A survey of blade tip-timing measurement techniques for turbomachinery vibration," *J. Eng. Gas Turbines Power*, vol. 120, no. 4, pp. 784–791, Oct. 1998.

[9] Z. S. Chen, H. Sheng, Y. M. Xia, W. M. Wang, and J. He, "A comprehensive review on blade tip timing-based health monitoring: Status and future," *Mech. Syst. Signal. Process.*, vol. 149, Feb. 2021, Art. no. 107330.

[10] B. Salhi, J. Lardies, and M. Berthillier, "Identification of modal parameters and aeroelastic coefficients in bladed disk assemblies," *Mech. Syst. Signal. Process.*, vol. 23, no. 6, pp. 1894–1908, Aug. 2009.

[11] Z. S. Chen, Y. M. Yang, B. Guo, and H. Zheng, "Blade damage prognosis based on kernel principal component analysis and grey model using sub-sampled tip-timing signals," *Proc. Inst. Mech. Eng., C, J. Mech. Eng. Sci.*, vol. 228, no. 17, pp. 3178–3185, Mar. 2014.

[12] Z. S. Chen, Y. M. Yang, X. Yong, B. Guo, and H. Zheng, "Non-contact crack detection of high-speed blades based on principal component analysis and Euclidian angles using optical-fiber sensors," *Sens. Actuators A, Phys.*, vol. 201, no. 15, pp. 66–72, Oct. 2013.

[13] Z. S. Chen, J. He, and C. Zhan, "Undersampled blade tip-timing vibration reconstruction under rotating speed fluctuation: Uniform and nonuniform sensor configurations," *Shock Vib.*, vol. 2019, Aug. 2019, Art. no. 8103216.

[14] Z. S. Chen, J. H. Liu, C. Zhan, J. He, and W. M. Wang, "Reconstructed order analysis-based vibration monitoring under variable rotation speed by using multiple blade tip-timing sensors," *Sensors*, vol. 18, no. 10, p. 3235, 2018.

[15] J. Lin, Z. Hu, Z. S. Chen, Y. M. Yang, and H. L. Xu, "Sparse reconstruction of blade tip-timing signals for multi-mode blade vibration monitoring," *Mech. Syst. Signal Process.*, vol. 85, pp. 250–258, Dec. 2016.

[16] H. L. Xu, Z. S. Chen, Y. M. Yang, L. M. Tao, and X. F. Chen, "Effects of crack on vibration characteristics of mistuned rotated blades," *Shock Vib.*, vol. 2017, Feb. 2017, Art. no. 1785759.

[17] D. L. Donoho, "Compressed sensing," *IEEE Trans. Inf. Theory*, vol. 52, no. 4, pp. 1289–1306, Jan. 2006.

[18] H. L. Xu, Z. S. Chen, Y. M. Yang, and L. M. Tao, "Multi-band blade vibration monitoring by blade tip-timing method based on compress sensing," in *Proc. 1st World Congr. Condition Monit.*, 2017, pp. 481–491.

[19] Z. S. Chen, H. Sheng, and Y. M. Xia, "Multi-coset angular sampling-based compressed sensing of blade tip-timing vibration signals under variable speeds," *Chin. J. Aeronaut.*, vol. 34, pp. 83–93, Sep. 2021.

[20] M. H. Pan, F. J. Guan, H. F. Hu, Y. M. Yang, and H. L. Xu, "Compressed sensing based on dictionary learning for reconstructing blade tip timing signals," in *Proc. Prognostics Syst. Health Manag. Conf. (PHM-Harbin)*, Jul. 2017, pp. 1–7.

[21] R. P. Spada and R. Nicoletti, "Applying compressed sensing to blade tip timing data: A parametric analysis," in *Proc. 10th Int. Conf. Rotor Dyn.* Cham, Switzerland: Springer, 2018, pp. 121–134.

[22] J. Liang, L. J. Li, and C. K. Zhao, "A transfer learning approach for compressed sensing in 6G-IoT," *IEEE Internet. Things J.*, vol. 8, no. 20, pp. 15276–15283, Oct. 2021.

[23] P. Agrawal, D. Chaudhary, V. Madaan, A. Zabrovskiy, R. Prodan, D. Kimovski, and C. Timmerer, "Automated bank cheque verification using image processing and deep learning methods," *Multimedia Tools. Appl.*, vol. 80, pp. 5319–5350, Oct. 2021.

[24] V. Hadi and H. M. Armita, "Persian speech recognition using deep learning," *Int. J. Speech. Technol.*, vol. 23, pp. 893–905, Nov. 2020.

[25] E. Zisselman, A. Adler, and M. Elad, "Compressed learning for image classification: A deep neural network approach," in *Handbook of Numerical Analysis*. Amsterdam, The Netherlands: Elsevier, 2018, pp. 3–17.

[26] J. C. Ye and Y. S. Han, "Deep convolutional framelets: A general deep learning for inverse problems," *SIAM. J. Imaging. Sci.*, vol. 11, no. 2, pp. 991–1048, Jul. 2017.

[27] Y. K. Gu, L. Zeng, and G. Q. Qiu, "Bearing fault diagnosis with varying conditions using angular domain resampling technology, SDP and DCNN," *Measurement*, vol. 19, May 2020, Art. no. 107616.

[28] E. J. Candès, "The restricted isometry property and its implications for compressed sensing," *Comp. Rendus Math.*, vol. 346, nos. 9–10, pp. 589–592, May 2008.

[29] S. Ioffe and C. Szegedy, "Batch normalization: Accelerating deep network training by reducing internal covariate shift," in *Proc. 32nd Int. Conf. Mach. Learn.*, 2015, pp. 448–456.

[30] G. Chen, P. Chen, Y. Shi, C.-Y. Hsieh, B. Liao, and S. Zhang, "Rethinking the usage of batch normalization and dropout in the training of deep neural networks," 2019, *arXiv:1905.05928*.

[31] G. E. Hinton, N. Srivastava, A. Krizhevsky, I. Sutskever, and R. R. Salakhutdinov, "Improving neural networks by preventing co-adaptation of feature detectors," 2012, *arXiv:1207.0580*.

[32] S. Park and N. Kwak, "Analysis on the dropout effect in convolutional neural networks," in *Proc. Asian Conf. Comput. Vis.*, 2016, pp. 189–204.

[33] C. Y. Zhou, H. F. Hu, F. J. Guan, and Y. Yang, "Modelling and simulation of blade tip timing uncertainty from rotational speed fluctuation," in *Proc. Prognostics Syst. Health Manag. Conf. (PHM-Harbin)*, Jul. 2017, pp. 1–5.

[34] Z. S. Chen, Y. M. Xia, H. Sheng, and J. He, "Analysis and calibration of blade tip-timing vibration measurement under variable rotating speeds," *IEEE Access*, vol. 9, pp. 141467–141478, 2021.

[35] D. P. Kingma and J. Ba, "Adam: A method for stochastic optimization," 2014, *arXiv:1412.6980*.

[36] L. Han, L. G. Han, and Z. Li, "Inverse spectral decomposition with the SPGL1 algorithm," *J. Geophys. Eng.*, vol. 9, no. 4, pp. 423–427, Aug. 2012.

[37] W. M. Wang, X. L. Zhang, D. F. Hu, D. P. Zhang, and P. Allaire, "A novel none once per revolution blade tip timing based blade vibration parameters identification method," *Chin. J. Aeronaut.*, vol. 33, no. 7, pp. 1953–1968, Jul. 2020.

[38] D. L. Xu, L. Du, H. W. Liu, P. Wang, and J. Yan, "Compressive sensing of stepped-frequency radar based on transfer learning," *IEEE Trans. Signal Process.*, vol. 63, no. 12, pp. 3076–3087, Jun. 2015.

**ZHONGSHENG CHEN** (Member, IEEE) was born in Anhui, China, in 1977. He received the B.S., M.S., and Ph.D. degrees in mechanical engineering from the National University of Defense Technology, Changsha, China, in 1999, 2001, and 2004, respectively.

From 2004 to 2017, he was a Lecturer and an Associate Professor with the College of Mechatronic Engineering and Automation, National University of Defense Technology. From 2017 to 2022, he was a Professor with the College of Electrical and Information Engineering, Hunan University of Technology. Since July 2022, he has been a Professor with the College of Automotive Engineering, Changzhou Institute of Technology. His current research interests include embedded fault diagnosis and prognostics, condition monitoring, and nonlinear vibration energy harvesting.

**HAO SHENG** was born in Anhui, China, in 1994. He received the B.S. degree in electrical engineering from the Fuyang Normal College, in 2018, and the M.S. degree in electrical engineering from the Hunan University of Technology, in 2021. His research interest includes BTT vibration monitoring.

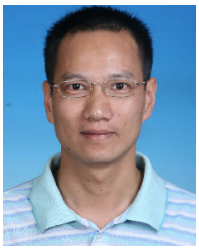

**LIANYING LIAO** was born in Fujian, China, in 1978. He received the B.S. and M.S. degrees in vehicle engineering from the Wuhan University of Technology, Wuhan, China, in 2001 and 2004, respectively, and the Ph.D. degree in vehicle engineering from Jiangsu University, Zhenjiang, China, in 2018.

From 2004 to 2023, he was a Lecturer, an Associate Professor, and a Professor with the College of Automotive Engineering, Changzhou Institute of Technology. His current research interests include embedded fault diagnosis and prognostics, noise, and vibration reduction technology for vehicles.

**CHENGWU LIU** was born in Anhui, China, in 1975. He received the B.S. degree in automotive engineering from Fujian Agriculture and Forestry University, in 1998, and the Ph.D. degree in mechanical engineering from the Nanjing University of Science and Technology, in 2007.

From 2007 to 2021, he was a Lecturer, an Associate Professor, and a Professor with the College of Mechanical and Automotive Engineering, Fujian University of Technology. Since April 2021, he has been a Professor with the College of Automotive Engineering, Changzhou Institute of Technology. His current research interests include structural vibration and noise control and structural optimization.

**YEPING XIONG** is currently an Associate Professor with the Faculty of Engineering and Physical Sciences, University of Southampton, U.K. She has over 35 year's experiences in dynamics, vibration, and control. Prior to joining the University of Southampton, she has been a Professor in vibration engineering with Shandong University, since 1996. She has published over 190 papers. Her current research interests include structure dynamics, energy harvesting, smart material and structures, vibration control, and multidisciplinary optimization.